frontiers | Frontiers in Physics

TYPE Original Research
PUBLISHED 26 October 2023
DOI 10.3389/fphy.2023.1240468

Check for updates

OPEN ACCESS

EDITED BY
Yanyu Chen,
University of Louisville, United States

REVIEWED BY
Jacopo Maria De Ponti,
Polytechnic University of Milan, Italy
Chen Shen,
Rowan University, United States

*CORRESPONDENCE
Xinsa Zhao,
xinsazhao@163.com
Jianning Han,
hanjn46@nuc.edu.cn

†These authors have contributed equally to this work

RECEIVED 15 June 2023
ACCEPTED 09 October 2023
PUBLISHED 26 October 2023

CITATION
Zhang S, Hao G, Zhao X, Liu Y and Han J (2023), Broadband acoustic signal enhancement via gradient metamaterials coupled to crystals.
Front. Phys. 11:1240468.
doi: 10.3389/fphy.2023.1240468

COPYRIGHT
© 2023 Zhang, Hao, Zhao, Liu and Han. This is an open-access article distributed under the terms of the Creative Commons Attribution License (CC BY). The use, distribution or reproduction in other forums is permitted, provided the original author(s) and the copyright owner(s) are credited and that the original publication in this journal is cited, in accordance with accepted academic practice. No use, distribution or reproduction is permitted which does not comply with these terms.

Broadband acoustic signal enhancement via gradient metamaterials coupled to crystals

Sai Zhang[1†], Guodong Hao[2†], Xinsa Zhao[2*], Yexin Liu[2] and Jianning Han[2*]

[1]The Institute of Ultrasonic Testing, Jiangsu University, Zhenjiang, Jiangsu, China, [2]School of Information and Communication Engineering, North University of China, Taiyuan, Shanxi, China

In this work, a phononic crystal gradient metamaterial structure (PCGMs) is proposed based on the strong wave compression effect coupled with equivalent medium theory to achieve enhancement and directional sensing of weak target acoustic signals. Compared with the conventional gradient structure, PCGMs exhibit superior acoustic enhancement performance and wider range of acoustic response capability. Numerical analysis and experimental validation consistently demonstrate that PCGMs can effectively enhance the target frequency signals in harmonic signals. This study breaks through the detection limit of acoustic sensing systems and provides a great method for engineering applications of weak acoustic signal perception.

KEYWORDS

acoustic metamaterial, weak sound sensing, gradient structure, phononic crystal, impedance matching

1 Introduction

The application of weak acoustic signal enhancement technology has emerged as a crucial technological tool in the fields of hydroacoustic communication [1, 2], biomedicine [3], and environmental monitoring [4, 5]. Over the past decade, considerable progress has been achieved in enhancing the signal-to-noise ratio in electrical sensor device applications [6, 7]. Nonetheless, certain discriminative information within acoustic signals, such as harmonic signals arising from structural damage [8, 9], can be quite weak, often going unnoticed due to either falling below the microphone sensitivity threshold or being obscured by intense background noise. Therefore, it is imperative to devise an acoustic signal sensing system capable of effectively amplify weak acoustic signals.

In the last 2 decades, researchers have paid much attention to acoustically artificial metamaterials. By designing intricate acoustic metamaterials, they aim to control acoustic field information through negative mass density and negative bulk modulus properties [10–12]. New physical phenomenon and mechanisms such as sound absorption [13, 14], focusing [15–17], directional transmission [18–20], and acoustic rainbow trapping [21–26] have been generated. Compared with conventional acoustic materials, Zhu et al. [27] first proposed a subwavelength gradient grid-type structure that employs subwavelength gaps to selectively capture acoustic signals across various frequency bands. This innovation demonstrates the structure's capability to modulate the spatial distribution of acoustic energy. Chen et al. [28] performed a systematic theoretical analysis of gradient acoustic metamaterial structures (GAMs). Huang et al. [29] developed an improved gradient structure acoustic metamaterials (AMMs) featuring

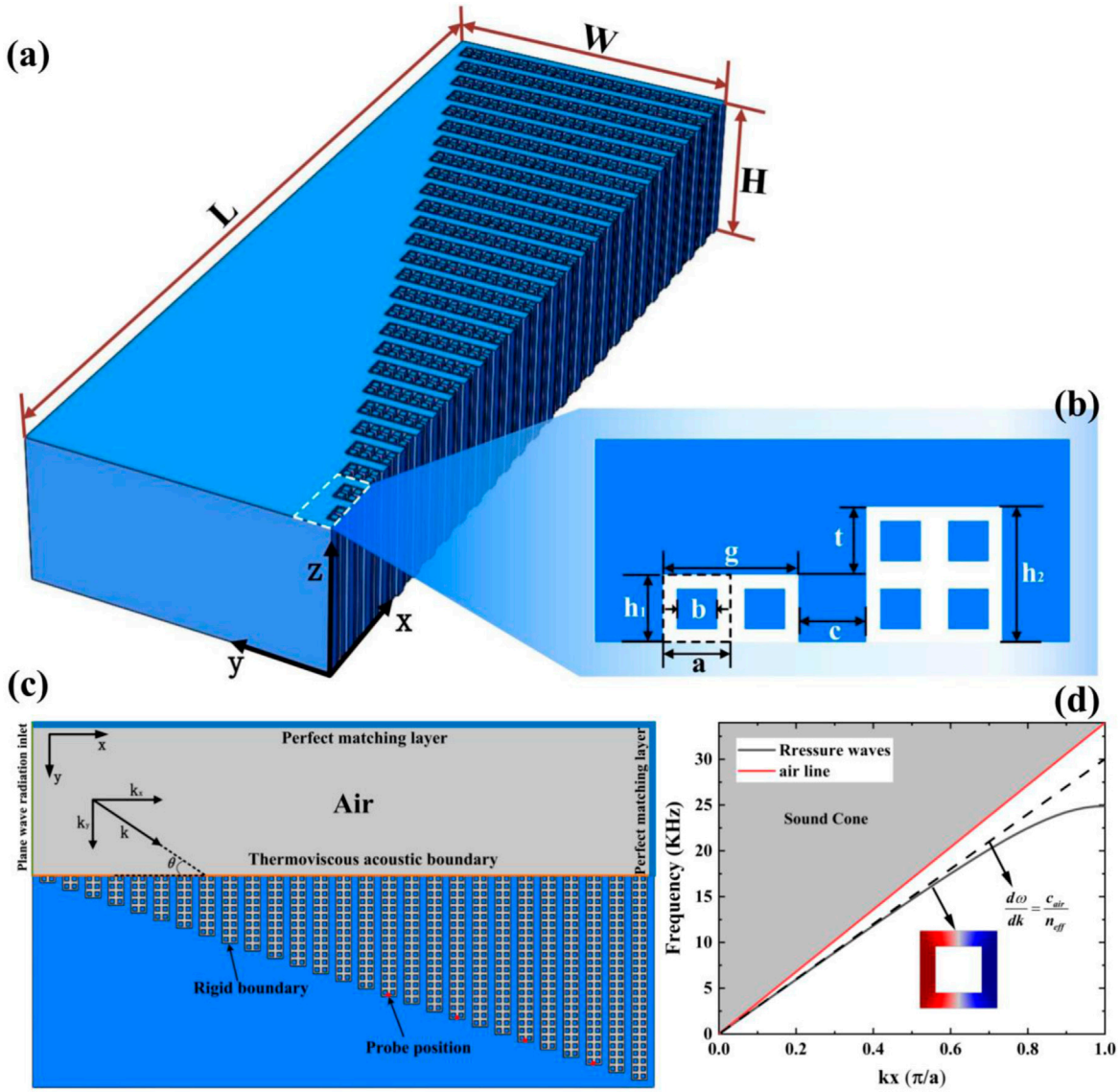

FIGURE 1
(A) Simulated acoustic system of PCGMs; **(B)** enlarged view of two gap structures; **(C)** two-dimensional structure of PGCMs; **(D)** dispersion diagram.

gradient profiles, varying thickness, and gap width, which resulted in a significant acoustic gain of more than an order of magnitude. Recently Chen [30] introduced a gradient metamaterial coupled with spacing-coiling structure, which has the potential to amplify acoustic signals by approximately 80 times within the lower frequency range. However, the frequency bandwidth of the acoustic signal captured by each slit is reduced, and the frequency band blind area between the gaps of the gradient structure is increased, making it less suitable for practical engineering applications. Furthermore, we discovered that high refractive index media features can be constructed using subwavelength phononic crystal (PC) arrays [31, 32]. Nejad [33] created an acoustic fiber with a higher refractive index than uniform air using cross-shaped phononic crystals. Ruan [34] and Ahmed Allam [35] constructed 2D and 3D phononic crystal focusing lenses based on the equivalent gradient refractive index feature possessed by gradient phononic crystals for applications in underwater acoustic focusing.

In this work, we incorporate phononic crystals to enhance the gradient metamaterial properties. Phononic crystal gradient metamaterial structures (PCGMs) were designed and constructed using photosensitive resin. In contrast to traditional gradient metamaterials, PCGMs offer superior acoustic enhancement and a broader range of response angles, without loss of bandwidth of the captured acoustic signal per gap. Experimental test results demonstrate that PCGMs exhibit superior acoustic response capabilities when detecting harmonic acoustic signals.

TABLE 1 Summary of characteristic parameters.

Parameters	h_1	h_2	g	c	t	b	a	H	L	W
Values (mm)	5	10	10	5	5	3	5	70	410	140

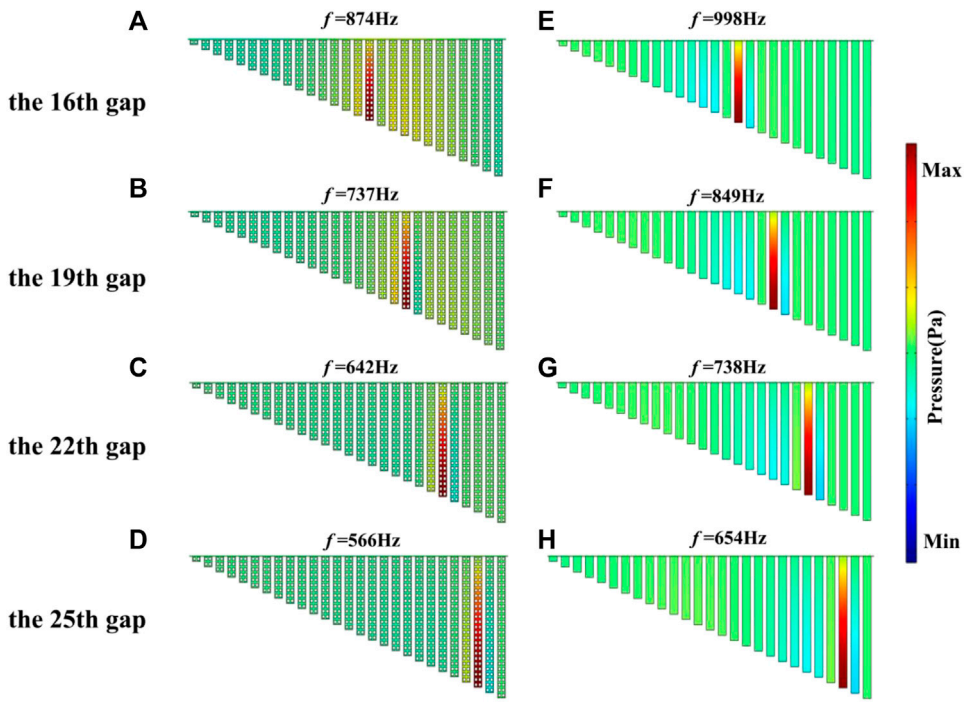

FIGURE 2
Simulation results of sound pressure distribution of two structures at different frequencies: **(A–D)** PGCMs structure; **(E–H)** GAMs structure.

2 Structural design

The phononic crystal gradient structures (PCGMs) designed and constructed in this paper are depicted in Figure 1A. Figure 1B provides an enlarged view of the two gaps with the relevant parameters labeled. The position of the lower left corner of the first plate is designated as the coordinate origin. The width of the first plate is set at e = 5 mm, while the widths of the 2nd to 27th rectangular plates increase uniformly by t = 5 mm. The plate thickness is c = 5 mm, and the gap between the plates is established at g = 10 mm. The height H of the sample is set to 70 mm. Within the structure's air gaps, phononic crystal units are formed by immersing a side b = 3 mm square solid at the center of the air region with a side a = 5 mm square. Each gap contains two rows of phononic crystal arrays, with adjacent gaps distinguished by two phononic crystals. All parameters are summarized and listed in Table 1.

3 Theoretical and numerical analysis

3.1 Theory

The effective mass density and bulk modulus of PCGMs can be obtained using the equivalent medium theory, which can be expressed as [36].

$$\rho = \frac{\rho_{res}\rho_{eff}}{(1-F_r)\rho_{res} + F_r\rho_{eff}} \tag{1}$$

$$K = \frac{K_{res}K_{eff}}{(1-F_r)K_{res} + F_rK_{eff}} \tag{2}$$

where F_r is the filling rate of the parallel plate. The constructed models of PCGMs are fabricated using photosensitive resins. The material has a density of $\rho_{res} = 1130kg/m^3$ and a bulk modulus of $K_{res} = 2.65GPa$. The air has a density of $\rho_{air} = 1.2kg/m^3$ and a bulk modulus of $K_{air} = 1.42 \times 10^5 Pa$. The PC structure between the two plates provides a larger propagation path for the sound than uniform air, effectively reducing the sound propagation velocity [37]. The calculated crystal band structure is shown in Figure 1D, where the lowest band is located below the sound cone (gray part). The coefficient of reduction of the equivalent speed of sound between the two plates c_{eff} (filling the PC structure) with respect to c_{air} (the speed of sound in air) can be expressed in terms of the effective refractive index. As illustrated in Figure 1D, the dispersion in the lowest frequency band is linear over a wide bandwidth from 0 to 13 kHz (indicated by the dashed line). The slope k of this linear fit is

$$k = c_{air}\big/\left(2\pi \cdot n_{eff}\right) \tag{3}$$

where n_{eff} is the effective refractive index of the PC. In addition, the effective refractive index of the PC medium constructed between the two plates in this band range is higher than that of uniform air (n_{eff} = 1.17 > 1). This is the key factor that PCGMs can enables PCGMs to improve the refractive index of GAMs. The function of PCGMs width can be expressed as

$$z(x) = tx/(c+g) + h_1/3 \tag{4}$$

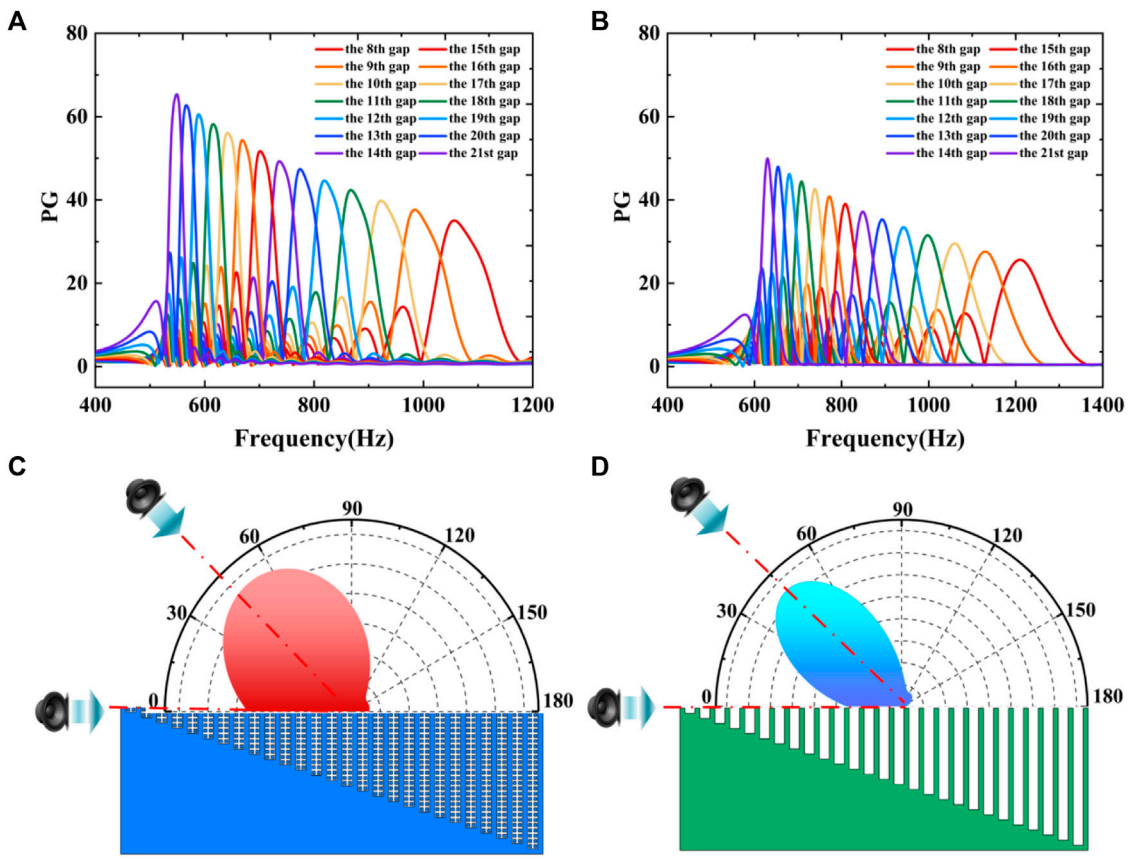

FIGURE 3
(A) Absolute sound pressure gain between different air gaps of PCGMs structure; **(B)** Absolute sound pressure gain between different air gaps of GAMs structure; **(C)** Polar plot of maximum absolute total sound pressure gain of PCGMs; **(D)** Polar plot of maximum absolute total sound pressure gain of GAMs.

The effective refractive index of the metamaterial can be derived as follows:

$$N_{PCGM}(x,f) = \sqrt{n_{eff} + \frac{K_{eff}\cdot\rho_{eff}}{\rho\cdot K}}\left(\tan\left[2\pi f\cdot\frac{z(x)}{2}\cdot\sqrt{\frac{\rho}{K}}\right]\right)^2 \tag{5}$$

where K_{eff} represents the equivalent bulk modulus of PC, and ρ_{eff} represents the equivalent density of PC. Simultaneously,

$$\frac{K_{eff}\rho_{eff}}{\rho\cdot K} \approx (1-F_r)^2 \tag{6}$$

F_r increases linearly with the x-axis direction of PCGMs, which is consistent with the characteristics of GAMs without the addition of PC structures. However, $\sqrt{\frac{\rho}{K}} \approx \sqrt{\frac{\rho_{eff}}{K_{eff}}} = c_{eff} < c_{air}$ leads to a reduction in the magnitude of refractive index variation per gap for PCGMs compared to GAMs.

As a result, n_{PCGM} exhibits a higher and more smoothly varying refractive index compared to that of conventional GAMs. The relationship between the sound pressure amplitude and the input frequency along the x-axis, according to the above equation, is:

$$P_{PCGM}(x,f) = \frac{\sqrt{2\pi\cdot\rho_{eff}f}\cdot\sqrt[4]{1-n_{PCGM}^{-2}}}{\cos\left[\arctan\left(\rho\cdot\rho_{eff}^{-1}\sqrt{n_{PCGM^{-1}}^{2}}\right)\right]} \tag{7}$$

Since PCGMs incorporate PC structure in the gap between the two plates compared to conventional GAMs, it results in an increase of n_{PCGM} and the PC equivalent density ρ_{eff}. Consequently, P_{PCGM} becomes larger.

The above theoretical examination of equivalent media demonstrates that PCGMs can effectively amplify acoustic signals. From a microscopic perspective, the propagation of sound waves in metamaterial structures is characterized by the presence of PC structures between the two baffles of gradient configurations. Simultaneously, different gaps capture acoustic signals with varying frequencies. The periodic structure of phononic crystals influences phonon propagation, resulting in the Bragg diffraction effect. This phenomenon is akin to Bragg diffraction in photonic crystals, which restricts the propagation of sound waves in specific directions, consequently increasing the refractive index of the sound waves. Additionally, when sound waves are reflected and scattered in phononic crystals, various wave paths generate interference effects. In certain instances, this interference can enhance the amplitude of sound waves, thereby increasing their energy density. On one side,

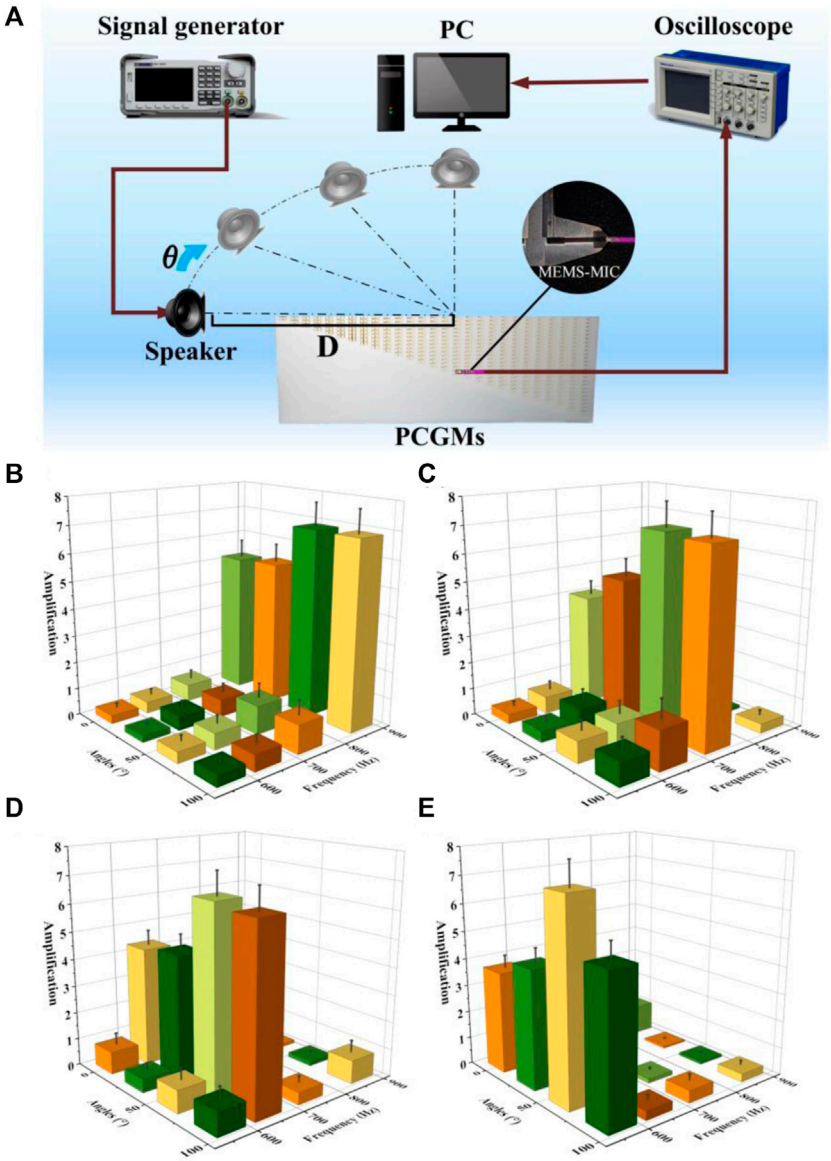

FIGURE 4
(A) Test system based on PCGMs Maximum spectral amplitude of target frequencies corresponding to different gaps **(B)** 16 gap **(C)** 19 gap **(D)** 22 gap **(E)** 25 gap.

sound waves reach the central gap of the structure through a convoluted configuration, forming a resonance with the rigid boundary at the end of the gap, which further amplifies the amplitude. Furthermore, the PC structure between each gap reduces the operating frequency captured by PCGMs compared to GAMs per gap.

3.2 Numerical analysis

Considering the characteristics of the PCGMs constructed as described above, we perform numerical simulations to analyze their performance. In the simulation environment, the structure can be regarded as a two-dimensional (2D) acoustic system. In order to consider the viscoelastic and dissipative problems faced by the acoustic energy transmission in the structure, we added a thermo-viscous boundary layer impedance in the pressure acoustics module, set the acoustic energy transmitted in air with a kinetic viscosity of 1.85×10^{-5} and a body viscosity of 1.11×10^{-5}, and the thermal conditions were set to be adiabatic, and thus simulated the data to be as close as possible to the real data. Accordingly, we build a 2D structure within the acoustic module (pressure acoustics and thermo-viscous acoustics) of COMSOL Multiphysics v6.0, as illustrated in Figure 1C, with the point probe positions set at the locations marked in red (16th, 19th, 22nd, and 25th air gaps). The pressure gain value (PG) is an important indicator of the acoustic enhancement effect, defined as PG = PM/PF [28, 38]. PM denotes the sound pressure amplitude added to the metamaterial structure, while PF indicates the sound pressure amplitude in the free sound field. To compare the impact of the PC structure on the acoustic enhancement of the

gradient structure, the conventional GAMs structure [27] is constructed by removing the PC structure in the above designed simulation environment. We perform frequency domain analysis simulations for both PCGMs and GAMs.

Figures 2A–D show that the center frequencies of the 16th, 19th, 22nd and 25th air gaps of the PCGMs structure are 874 Hz, 737 Hz, 642 Hz and 566 Hz, respectively. For comparative analysis, Figure 2E–H display the sound pressure distribution at the center frequency for the GAMs structure at the same gap positions. Figures 3A, B further calculate the absolute acoustic pressure frequency response obtained from the simulation of the PCGMs structure and the GAMs structure without the addition of phononic crystals for different air gaps (from the 8th air gap to the 21st air gap). The amplified sound pressure amplitudes of the 16th, 19th, 22nd, and 25th air gaps in the PCGMs structure were 42.4, 49.3, 56, and 62.7 times, respectively. In the GAMs structure, the amplified sound pressure amplitudes for the same selected air gaps were 31.45, 37.2, 42.6, and 48 times, respectively. Compared to the GAMs structure, the proposed PCGMs structure in this paper captures a lower frequency, approximately 15.7% lower. In the traditional sense of gradient materials, capturing a lower frequency of the acoustic signal typically requires a larger volume for the gradient structure. The characteristics of the structure can effectively address the issue of gradient structure to cope with the detection of low-frequency signals and large volume. This provides an important solution for the practical application of gradient structures. In addition, it can also be observed that the average absolute sound pressure amplification gain increases by 30.3% for the PCGMs structure compared to the GAMs structure.

The polar normalized plots of the maximum absolute total acoustic pressure gain of the metamaterial waveguide obtained through finite element simulations are illustrated in Figures 3C, D. The waveguide of the PCGMs structure demonstrates significant directionality. Under ideal conditions, the acoustic source is incident at the top left of the PCGMs toward the 51.1° position. In this scenario, the acoustic waves can achieve optimal coupling within the PCGMs waveguide, while the best coupling angle for the conventional GAMs structure is 39.6°. The inclusion of the PC structure causes the optimal coupling angle of the gradient structure to increase. At greater or less than the optimal coupling angle, both structures exhibit a gradual weakening of the response with angle change. Figure 3C also distinctly demonstrates that PCGMs possess a broader angular response range compared to the GAMs.

4 Experimental verification

To evaluate the perceptual performance of the proposed PCGMs structure in response to the actual special signals, an experiment is conducted in this study. The harmonic signals emitted by the speaker are:

$$P(t) = \cos(2\pi \times f_0 \times t) + \cos(2\pi \times f_1 \times t) + \cos(2\pi \times f_2 \times t) + \cos(2\pi \times f_3 \times t) \quad (8)$$

The target frequencies f0 = 566 Hz, f1 = 642 Hz, f2 = 737 Hz, and f3 = 874 Hz correspond to the operating center frequencies of the 16th, 19th, 22nd, and 25th air gaps, respectively. A test system based on PCGMs was constructed, as depicted in Figure 4A. The speaker is positioned at a distance of D = 0.7 m from the PCGMs location. Starting from the vertical speaker position angle of the PCGMs, the angle θ is rotated clockwise to observe the voltage signals collected by the MEMS-MIC at varying angles. The sound measurement device utilized in this paper is a MEMS-MIC (model: S15OT421-005, sensitivity: −42 dB, amplification gain of 66), which is placed at the end edge of the gap to detect the sound signal.

The acoustic signal responses for the 16th, 19th, 22nd, and 25th air gaps are acquired using the MEMS-MIC. The maximum spectral amplitudes of the target frequencies corresponding to the different gaps, obtained by varying the angle θ (0°, 30°, 60°, and 90°) of the sound source relative to the PCGMs structure, are depicted in Figure 4B–E. It is evident that each gap displays strong target selectivity, enabling amplification for the target frequency. However, this amplification function is not realized for signals in other frequency bands. Moreover, by comparing the acoustic signal response obtained from the four gaps at various source angles, we can clearly find that from $\theta = 0°$, the acoustic response capability of the four gaps gradually improves as the angle increases. The optimal amplification effect is achieved when the sound source is at an angle of 60° from the structure of PCGMs. With the increase of θ value, the amplitude of the PCGMs' response to the target frequency signal gradually diminishes. When the source is at $\theta = 90°$ from the PCGMs, the PCGMs still have a certain enhanced response to the target frequency signal. This observation aligns with the gain polar curve obtained from the simulation.

5 Conclusion

In this work, we propose a PCGMs structure that leverages the strong wave compression effect in conjunction with the equivalent medium mechanism of phononic crystals to boost the amplitude of weak acoustic signals at the target frequency. The proposed PCGMs structure demonstrates superior performance in amplifying acoustic signal amplitudes compared to gradient models without the incorporation of PC structures. Furthermore, each slit within the structure possesses a working bandwidth that is on par with traditional gradient structures, thereby increasing the structure's practicality. Additionally, the PCGMs structure exhibits a broader angular range of acoustic response capabilities along with anisotropic features, which contribute to its enhanced efficiency in weak acoustic signal localization scenarios.

Looking ahead, we anticipate that PCGMs will flourish in practical engineering applications—particularly in the context of detecting target signals amidst complex environmental noise—due to their distinct advantages.

Data availability statement

The raw data supporting the conclusion of this article will be made available by the authors, without undue reservation.

Author contributions

SZ: funding acquisition and original draft. GH: experiment implementation, modeling, FEA, and original draft. XZ:

prototype fabrication, and editing. YL: experiment implementation. JH: funding acquisition and supervised the research. All authors contributed to the article and approved the submitted version.

Funding

This work was in part by the Natural Science Foundation of Shanxi Province under Grants 202103021224201, the National Natural ScienceFoundation of China under Grant No. 62271235, the Foundation of State Key Laboratory of Dynamic Testing Technology under Grant No. 2022-SYSJJ-10, and the Graduate Science and Technology Project of North University of China under Grant No.20221835.

Conflict of interest

The authors declare that the research was conducted in the absence of any commercial or financial relationships that could be construed as a potential conflict of interest.

Publisher's note

All claims expressed in this article are solely those of the authors and do not necessarily represent those of their affiliated organizations, or those of the publisher, the editors and the reviewers. Any product that may be evaluated in this article, or claim that may be made by its manufacturer, is not guaranteed or endorsed by the publisher.

References

1. Bu FF, Luo HJ, Ma SS, Li X, Ruby R, Han GJ. AUV-aided optical—acoustic hybrid data collection based on deep reinforcement learning. *Sens* (2023) 23:578. doi:10.3390/s23020578

2. Sun ZY, Shi Y, Sun XC, Jia H, Jin ZK, Deng K, et al. Underwater acoustic multiplexing communication by pentamode metasurface. *J Phys D: Appl Phys* (2021) 54: 205303. doi:10.1088/1361-6463/abe43e

3. Zhao XS, Han JN, Yang P, Zhao RR. Research on high-efficiency transmission characteristics of multi-channel breast ultrasound signals based on graphene structure. *Crystals* (2021) 11:507. doi:10.3390/cryst11050507

4. Zhang HB, Zhang SB, He QB, Kong FR. The Doppler Effect based acoustic source separation for a wayside train bearing monitoring system. *J SOUND VIB* (2016) 361: 307–29. doi:10.1016/j.jsv.2015.09.038

5. Liu Z, He QB, Li ZW, Peng ZK, Zhang WM. Vision-based moving mass detection by time-varying structure vibration monitoring. *IEEE Sens J* (2020) 20:11566–77. doi:10.1109/jsen.2020.2998285

6. Rahaman A, Park CH, Kim B. Design and characterization of a MEMS piezoelectric acoustic sensor with the enhanced signal-to-noise ratio. *Sens Actuator A Phys* (2020) 311:112087. doi:10.1016/j.sna.2020.112087

7. Kryszyn J, Wanta DM, Smolik WT. Gain adjustment for signal-to-noise ratio improvement in electrical capacitance tomography system EVT4. *IEEE Sens J* (2017) 17: 8107–16. doi:10.1109/jsen.2017.2744985

8. Bovsunovsky A, Nosal O. Highly sensitive methods for vibration diagnostics of fatigue damage in structural elements of aircraft gas turbine engines. *Proced Struct Integrity* (2022) 35:74–81. doi:10.1016/j.prostr.2021.12.050

9. Yin TY, Ng C-T, Kotousov A. Damage detection of ultra-high-performance fibre-reinforced concrete using a harmonic wave modulation technique. *Constr Build Mater* (2021) 313:125306. doi:10.1016/j.conbuildmat.2021.125306

10. Zhang T, Bok E, Tomoda M, Matsuda O, Guo JZ, Liu XJ, et al. *Appl Phys Lett* (2022) 120:161701.

11. Chen HJ, Zeng HC, Ding CL, Luo CR, Zhao XP. *J Appl Phys* (2013) 46:475105.

12. Lee SH, Park CM, Seo YM, Wang ZG, Kim CK. Composite acoustic medium with simultaneously negative density and modulus. *Phys Rev Lett* (2010) 104:054301. doi:10.1103/physrevlett.104.054301

13. Liu L, Xie LX, Huang WC, Zhang XJ, Lu MH, Chen YF. *Appl Phys Lett* (2022) 120:251701.

14. Comandini G, Khodr C, Ting VP, Azarpeyvand M, Scarpa F. *Appl Phys Lett* (2022) 120:061902.

15. Tong SS, Ren CY, Tao J, Jiang LX. Broadband flattened underwater acoustic Luneburg lens. *J Phys D: Appl Phys* (2023) 56:025102. doi:10.1088/1361-6463/aca165

16. Dahmani H, Smagin N, Campistron P, Carlier J, Toubal M, Nongaillard B. *Appl Phys Lett* (2023) 122:102201.

17. Chen DC, Zhu XF, Wei Q, Yao J, Wu DJ. Broadband tunable focusing lenses by acoustic coding metasurfaces. *J Phys D: Appl Phys* (2020) 53:255501. doi:10.1088/1361-6463/ab8247

18. Lan J, Wang T, Zhao Y, Liu XZ, Wan XL, Liu YP, et al. Realization of real-time directional radiation of acoustic wave with non-uniform Mie resonators. *Appl Phys Express* (2022) 15:034001. doi:10.35848/1882-0786/ac4ecb

19. Sun JH, Wu TT. *Phys Rev B* (2006) 74:174305.

20. Dai HQ, Liu TT, Xia BZ, Yu DJ. Quasilossless acoustic transmission in an arbitrary pathway of a network. *Phys Rev B* (2017) 95:054109. doi:10.1103/physrevb.95.054109

21. Xu BQ, Wu J, Lu W, Gu X, Zhang LJ, Zhang S, et al. *J Appl Phys* (2021) 129:154501.

22. Wu HW, Yin YQ, Sheng ZQ, Li Y, Qi DX, Peng RW. Multiband omnidirectional ventilated acoustic barriers based on localized acoustic rainbow trapping. *Phys Rev Appl* (2021) 15:054033. doi:10.1103/physrevapplied.15.054033

23. Tsakmakidis KL, Boardman AD, Hess O. *Nature* (2007) 450:7168.

24. Colombi A, Colquitt D, Roux P, Guenneau S, Craster RV. A seismic metamaterial: the resonant metawedge. *Sci Rep* (2016) 6:27717. doi:10.1038/srep27717

25. De Ponti JM, Colombi A, Ardito R, Braghin F, Corigliano A, Craster RV. Graded elastic metasurface for enhanced energy harvesting. *New J Phys* (2020) 22:013013. doi:10.1088/1367-2630/ab6062

26. De Ponti JM, Iorio L, Riva E, Braghin F, Corigliano A, Ardito R. Enhanced energy harvesting of flexural waves in elastic beams by bending mode of graded resonators. *Front Mater* (2021) 8. doi:10.3389/fmats.2021.745141

27. Zhu J, Chen YY, Zhu XF, Garcia-Vidal FJ, Yin XB, Zhang WL, et al. Acoustic rainbow trapping. *Sci Rep* (2013) 3:1728. doi:10.1038/srep01728

28. Chen YY, Liu HJ, Reilly M, Bae H, Yu M. Enhanced acoustic sensing through wave compression and pressure amplification in anisotropic metamaterials. *Nat Commun* (2014) 5:5247. doi:10.1038/ncomms6247

29. Huang XJ, Yan YT, Ma JY, Li J, Rui XB. *IEEE Sens J* (2020) 20:4413.

30. Chen TG, Jiao JR, Yu DJ. Enhanced broadband acoustic sensing in gradient coiled metamaterials. *J Phys D: Appl Phys* (2021) 54:085501. doi:10.1088/1361-6463/abc6d7

31. Han JN, Hao GD, Yang WY, Zhao XS. Phononic crystal coupled mie structure for acoustic amplification. *Crystals* (2023) 13:1196. doi:10.3390/cryst13081196

32. Zhao XS, Hao GD, Shang Y, Han JN. Three-dimensional gradient metamaterial devices coupled with phononic crystals for acoustic enhancement sensing. *Crystals* (2023) 13:1191. doi:10.3390/cryst13081191

33. Zangeneh-Nejad F, Fleury R. Acoustic analogues of high-index optical waveguide devices. *Sci Rep* (2018) 8:10401. doi:10.1038/s41598-018-28679-1

34. Ruan YD, Liang X. 2D phononic-crystal Luneburg lens for all-angle underwater sound localization. *Acta Acust* (2022) 6:12. doi:10.1051/aacus/2021058

35. Allam A, Sabra K, Erturk A. 3D-Printed gradient-index phononic crystal lens for underwater acoustic wave focusing. *Phys Rev Appl* (2020) 13:064064. doi:10.1103/physrevapplied.13.064064

36. Huang SQ, Lin YB, Tang WJ, Deng RF, He QB, Gu FS, et al. *Front Phys* (2022) 10: 1027895.

37. Kock WE, Harvey F. Refracting sound waves. *J Acoust Soc Am* (1949) 21:471–81. doi:10.1121/1.1906536

38. Hao GD, Zhao XS, Han JN. A nonlinear gradient-coiling metamaterial for enhanced acoustic signal sensing. *Crystals* (2023) 13:1291. doi:10.3390/cryst13081291